Turkish Journal of Electrical Engineering & Computer Sciences

http://journals.tubitak.gov.tr/elektrik/

Research Article

Turk J Elec Eng & Comp Sci
(2017) 25: 3455 – 3467

doi:10.3906/elk-1611-23

Axial flux PM BLDC motor design methodology and comparison with a radial flux PM BLDC motor

Ertuğrul YEŞİLBAĞ[1], **Yasemin ERTUĞRUL**[2], **Lale ERGENE**[1,*]
[1]Department of Electrical Engineering, Faculty of Electrical and Electronic Engineering,
İstanbul Technical University, İstanbul, Turkey
[2]Informatics Institute, İstanbul Technical University, İstanbul, Turkey

Received: 03.11.2016 • **Accepted/Published Online:** 05.02.2017 • **Final Version:** 30.07.2017

Abstract: The aim of this paper is to develop a methodology to design an axial flux permanent magnet brushless direct current (AFPM) motor for a washing machine and compare the results with a conventional radial flux permanent magnet brushless direct current (RFPM) motor with the same power ratings. The AFPM motor is designed based on the maximum power density for an optimum inner-to-outer diameter ratio by using the reference RFPM motor constraints, such as the same rated torque at the rated speed. Both motors use the same materials in terms of lamination, permanent magnet, and conductor. They both use ferrite magnets; however, the AFPM motor has a surface-mounted structure and the RFPM motor has a buried one. The algorithm is used to determine the motor dimensions such as motor diameters, lengths, and the number of turns. The optimum number of poles considered for the design is chosen. Both motors are analyzed by finite element method (FEM) to verify the analytical approach and are compared in terms of power density, torque density, total weight and volume, torque ripple, and efficiency.

Key words: Permanent magnet machines, brushless motors, finite element analysis, electric motors, AC motors

1. Introduction

The axial flux principle was first used in Faraday's disc generator in 1831 [1]. This type of machine type would not be popular for a long time because of the lack of the material and the manufacturing technologies. Later on, developments in material technology, such as the production of a new generation of permanent magnets, and progress in power electronics provided new types of axial flux permanent magnet (AFPM) motor designs. Nowadays these motors are preferred in direct-drive traction applications because of their wide speed range operation capacity and compact structure [2–5]. For the same electrical performance indicators, AFPM motors have lower axial length, less weight, and a more compact structure. Thus, AFPM motors became a major competitor of radial flux permanent magnet (RFPM) motors. There are various studies comparing AFPM and RFPM motors. Some comparisons are performed by using the general sizing equations. Geometrical parameters, such as diameter and stack length, and electrical/magnetic parameters of the motor are considered for comparison. Those papers proved that AFPM motors are superior to RFPM motors in terms of torque/mass and power/volume ratio properties [6–12]. In one of these studies, a conventional RFPM motor was compared to four different axial flux topologies at five different power ratings regarding some construction and performance features such as required copper, steel weight, magnet weight, power per unit active weight, and torque per unit

*Correspondence: ergenel@itu.edu.tr

moment of inertia [9]. According to that study, AFPM motors offer higher power density and lower iron weight at the same power ratings, whereas the rotor inertia of RFPMs is higher than that of AFPM motors. However, a more complicated construction and higher windage losses in high speed applications are the disadvantages of these motors [10].

In this paper, a RFPM motor with 24/4 slot/pole that is currently used in a washer is used as a reference motor. For the given motor specification of an RFPM motor, a single-sided 12/8 slot/pole AFPM motor is designed optimally using the maximum point of power density obtained by a general sizing algorithm created in MATLAB. Analytical methods are used to determine the single-sided AFPM motor dimensions and also to calculate the volume, weight, losses, and efficiency of the RFPM and AFPM motors. Analytical and numerical results of both motors are compared in terms of power density, torque density, weight, volume, torque ripple, material weight, volume, and efficiency under the same output ratings as the output torque, output power and speed.

2. RFPM motor

The RFPM motor specifications currently used in washing machine application are 70 W, 1.2 Nm, 530 $\min^{-1}$, 230 V, 50 Hz. RFPM motor has 24 slots, 4 buried ferrite magnet poles, and single-layer lap winding. The number of series turns per phase is 292. Finite element analysis is preferred for the numerical simulations [13]. The RFPM motor is modeled in the finite element method (FEM)-based package program FLUX2D using given specifications and motor dimensions, and then the whole geometry is meshed to be ready for the analysis. The quarter of the RFPM motor layout and its mesh are given in Figure 1. The mesh consists of 18,540 line and 20,580 surface elements. The mesh is concentrated around the air gap where the flux values change rapidly. After construction of 2D geometric model of the RFPM motor, materials and physical quantities are defined. M700 steel is used as ferromagnetic material. The motor is driven by an inverter circuit that contains six IGBT transistors and six freewheeling diodes under the load operation. After materials and physical definition, the boundary conditions are also defined.

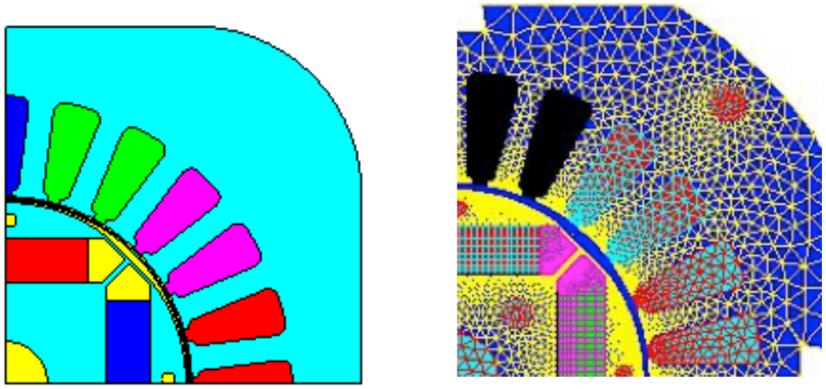

Figure 1. Quarter view of the RFPM motor and its mesh.

The RFPM motor numerical analyses include no-load and full-load operation conditions. No-load operation is achieved with the open-circuited stator phase windings, which means there is no stator current and the motor is rotated at a rated speed of 530 $\min^{-1}$. Back electromotor force (EMF) results from permanent magnets on the rotor measured from stator terminals. The full-load analysis of the RFPM motor is performed at a rated speed of 530 $\min^{-1}$. The RFPM motor is driven with an inverter circuit for the full-load operation.

The motor torque characteristic shows 1.26 Nm average shaft torque and 55% torque ripple according to FEM analysis. This average torque of motor is coherent with the test result of the 1.2 Nm rated shaft torque with a 5% relative error rate. The torque profile of the RFPM motor is given in Figure 2. The FEM result of induced back EMF waveforms at the rated speed is compared to that of the test result in terms of phase-to-phase peak value. The results are coherent, with a 2.21% relative error rate. The calculated and measured values are listed in Table 1. The numerical and experimental RFPM phase currents are obtained as 2.4 A and 2.43 A, respectively, with a 1.25% relative error rate. All results related to the no-load and full-load operation are presented in Table 1 [14]. The correlation between these results indicates the accuracy and consistency of FEM for analyzing the RFPM motor.

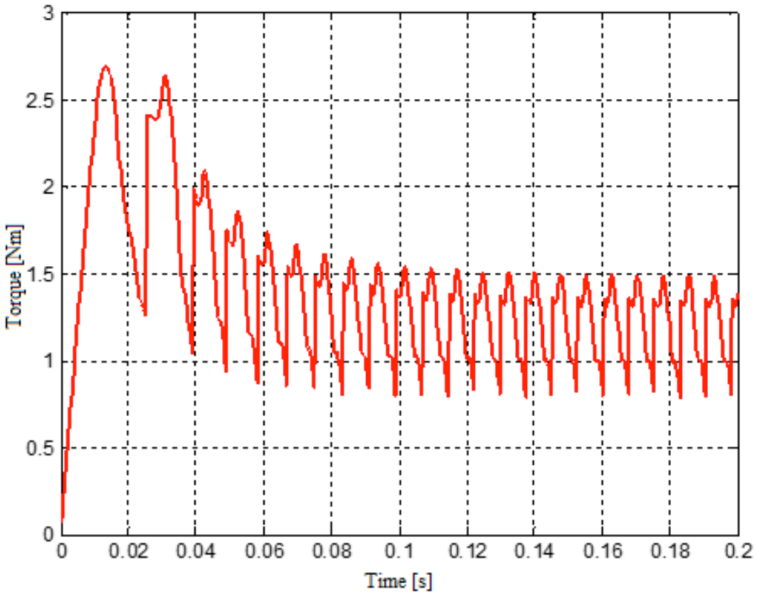

Figure 2. Torque characteristic of the RFPM motor at full load.

Table 1. Comparison of RFPM motor FEM and test results.

	FEM results	Test results	Relative error [%]
Back EMF [V]	22.6	23.11	2.21
Phase current [A]	2.43	2.4	1.25
Torque [Nm]	1.26	1.2	5

3. Methodology of AFPM motor design

In general, the AFPM motor is designed to be used instead of the RFPM motor in low-power washing machine applications. Axial flux motors have some advantages because of their disc shape, multistage capacity, high torque, and power density. These motors can be categorized into three types: single-sided (structure with one rotor and one stator), double-sided structure (one rotor between two stators or one stator between two rotors), and multistage structure (multiple stators with multiple rotors). The best topology of AFPM motor for low-power application is a single-sided (one rotor and one stator) slotted surface-mounted configuration to minimize weight, volume, and cost and to maximize power and torque density [8]. Moreover, single-sided motors have a less complicated structure than other AFPM motor layouts and have an easier manufacturing process.

3.1. Design of permanent magnet motor

Basic sizing equations are used to develop an algorithm in MATLAB that calculates axial flux motor main dimensions under the maximum power density conditions, changing the inner-to-outer diameter ratio for different numbers of poles [8–12]. The algorithm contains RFPM motors' rated output values, material characteristics, and electrical and magnetic loadings to ensure that the AFPM motor has the same operation characteristics as the RFPM motor. The same lamination steel, ferrite magnets, and copper conductor materials are used in the designed motor to make a proper comparison. The optimum number of poles is chosen and later the electrical design of AFPM motor is done. The design algorithm in MATLAB consists of sizing equations of the single-sided slotted surface-mounted AFPM motor. The output power of AFPM motor can be expressed as in Eq. (1) [10–12,15].

$$P_{out} = \frac{\pi}{2} K_e K_i K_p \eta B_g A_s \frac{f}{p} \left(1-\lambda^2\right) \left(\frac{1+\lambda^2}{2}\right) D_o^3 \tag{1}$$

In Eq. (1), K_e, K_i, K_p, η, B_g, A_s, f, p, λ, and D_o represent EMF factor, current factor, power waveform factor, efficiency, magnetic flux density in air gap, electrical loading, converter frequency, pole pair, motor inner-to-outer diameter ratio, and outer diameter, respectively. The factors in Eq. (1) are selected for a square wave drive [10–12,15]. In Eq. (1), the output power depends on λ and the number of pole pairs p and the effective volume of AFPM motor also depend on λ, which means that volumetric power density depends on λ and p. On the other hand, for a specific number of pole pairs, the power density depends on only λ and its maximum at a proper optimum λ value.

In Eq. (2), EMF peak value (E_{pk}) is calculated for AFPM. A reference peak value of EMF is taken into account from the RFPM machine and the number of turns and the outer diameter of motor are calculated. In Eq. (2), N_{Phase} and B_g are the number of turns per phase and air gap flux density, respectively.

$$E_{pk} = K_e N_{Phase} B_g \frac{f}{p} \left(1-\lambda^2\right) D_o^2 \tag{2}$$

The algorithm that sizes the AFPM motor also includes analytical equations given in Eqs. (3) to (9). D_g, L_{cu}, B_u, B_r, K_f, K_d, g, μ_r, L_{SM}, m, I_{rms}, and N_{Phase} are the average air gap diameter, the protrusion of the end winding from the iron stack in the radial direction, the attainable flux density on the surface of the permanent magnets, the residual flux density of permanent magnets, the flux focusing factor, the flux leakage factor of the permanent magnets, the air gap axial length, the recoil relative permeability of permanent magnets, the thickness of the permanent magnets in axial direction, the number of phase, the RMS current of stator phases, and the number of series turns of stator phases, respectively.

$$D_i = \lambda D_o \tag{3}$$

$$D_g = \frac{D_o(1+\lambda)}{2} \tag{4}$$

$$L_{cu} = \frac{\pi D_o \lambda}{8p} \tag{5}$$

$$K_f = \frac{B_g}{B_u} \tag{6}$$

$$K_d = 1 - \frac{p}{30} \tag{7}$$

$$L_{SM} = \frac{\mu_r B_g g}{(B_r - B_g)} \frac{K_f}{K_d} \tag{8}$$

$$N_{Phase} = \frac{A_s \pi D_g}{2mI_{rms}} \tag{9}$$

A flow chart of the AFPM motor design procedure is shown in Figure 3. The final process is using FEM to validate the design. If the design does not satisfy the requirements, then the algorithm changes the inner-to-outer diameter ratio and sizing in the AFPM motor for a different number of pole pairs.

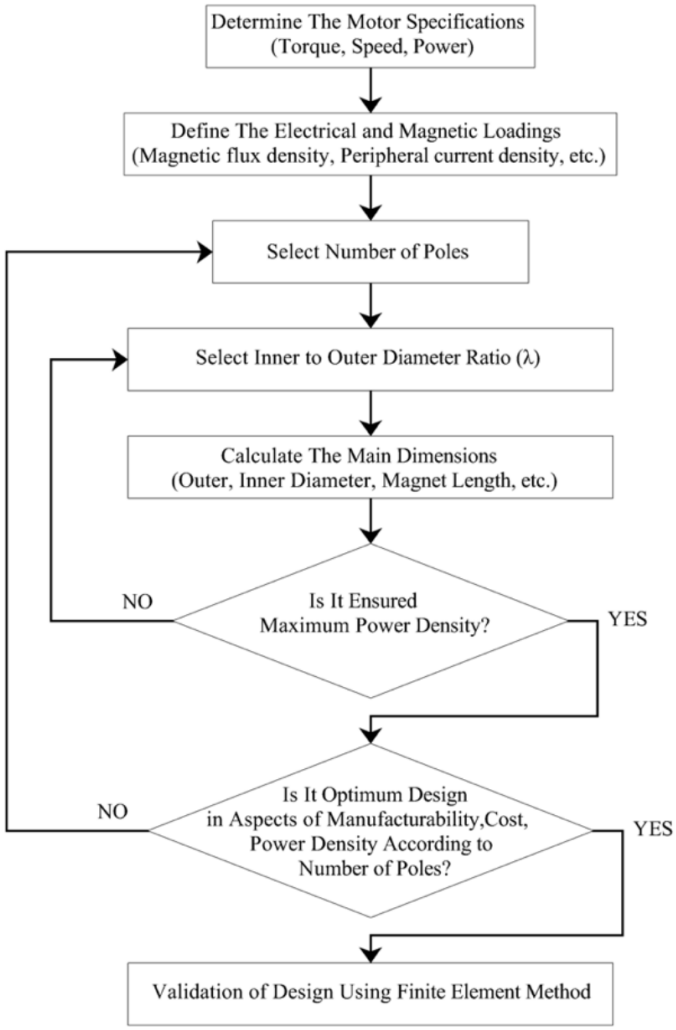

Figure 3. AFPM motor design flow chart.

Analytical AFPM motor design with a MATLAB algorithm are performed for six different numbers of poles initially (2, 4, 6, 8, 10, and 12). AFPM motor power density and torque density according to λ for different numbers of poles are shown in Figure 4. Each point in the curve represents a different AFPM motor

design. Power density is maximum at optimum λ for each pole pair (Figure 4). When λ is chosen properly, AFPM motor power density can be maximized. Torque density (the ratio of torque to motor weight) increases with λ (Figure 4).

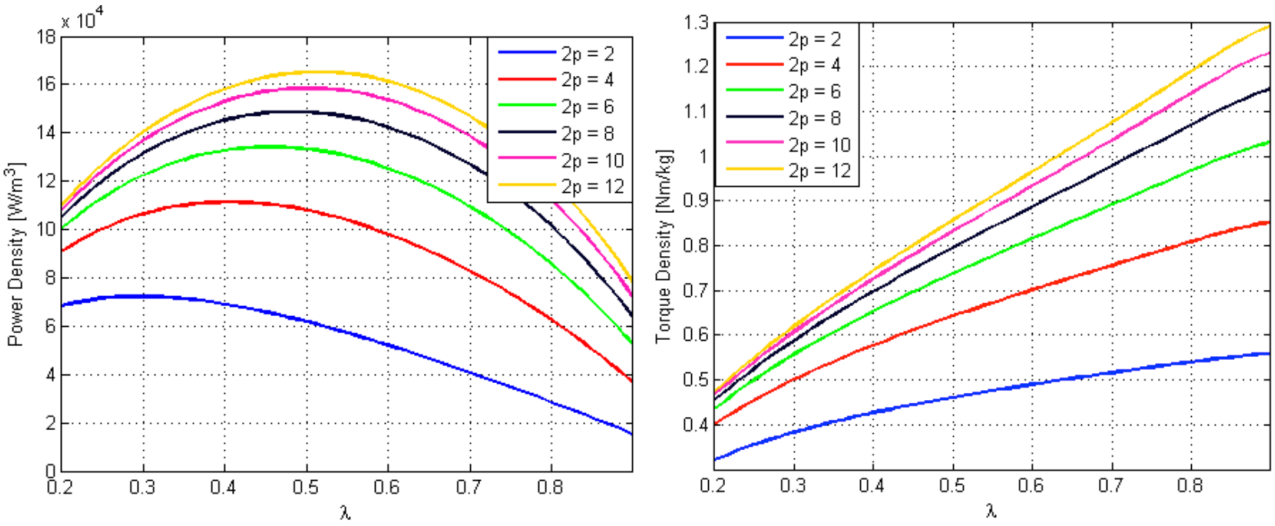

Figure 4. AFPM motor power density and torque density versus λ.

Figure 5 shows the motor volume and weight versus λ for different numbers of poles. The active volume versus λ curve has a local minimum point (Figure 5) that maximizes the power density of the AFPM motor (Figure 4). On the other hand, torque density increases with decreasing motor weight (Figure 5).

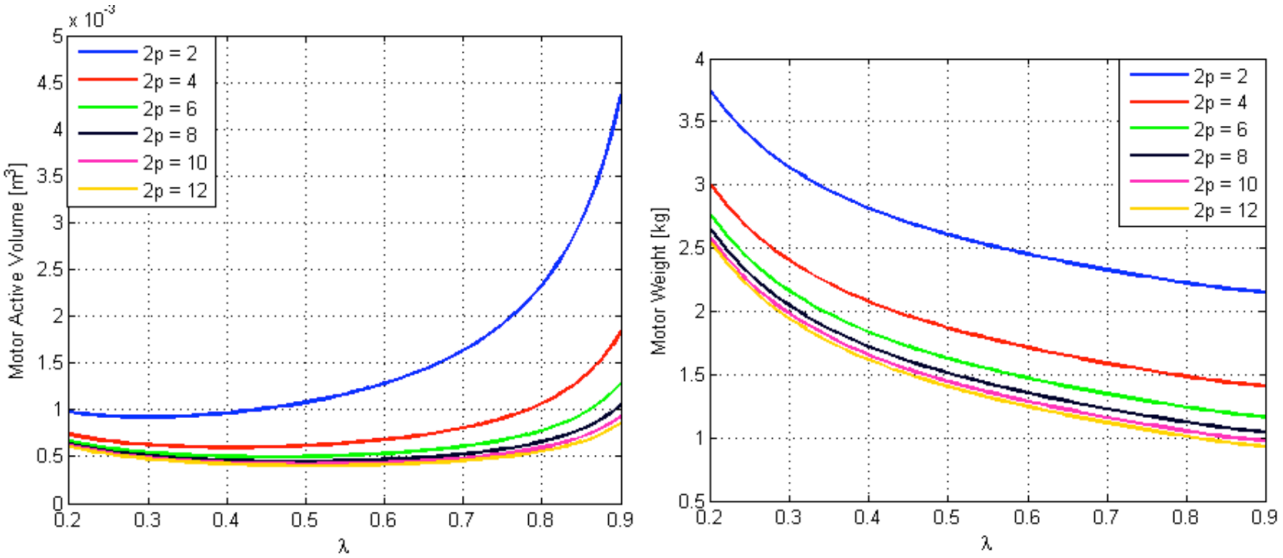

Figure 5. AFPM motor active volume and weight versus λ.

This study focuses on an AFPM motor design with higher power density, instead of an RFPM motor, because of the need for more compact washing machine motors. For this reason, the algorithm is also focused on maximizing power density with proper λ.

The algorithm for calculating maximum power density for different numbers of poles is shown in Table

2 with the other features of the designs. The volume and weight of designed AFPM motors do not decrease substantially up to pole number 8 (Table 2). The motor is driven with a high speed in the spinning operation, and the high speed requires high frequency and the need frequency increases with increasing number of poles. The higher frequency results in higher switching losses and a higher cost of switching equipment. In addition, more poles result in difficulties in magnet and motor production. Therefore, the optimum pole number with respect to the cost, manufacturability, and power density parameters is 8 (Table 2).

Table 2. The designed AFPM motor features for different numbers of poles.

Number of poles	Power density [kW/m^3]	Torque density [Nm/kg]	Volume [cm^3]	Weight [kg]	Optimum λ [Di/Do]
2	72.3	0.383	921.5	3.14	0.3
4	111.3	0.577	598.4	2.1	0.4
6	134.2	0.705	496.4	1.7	0.46
8	148.7	0.776	447.9	1.55	0.48
10	158.5	0.832	420.3	1.44	0.5
12	165.2	0.867	403.3	1.38	0.51

Afterwards, the single-side surface-mounted 8 pole AFPM motor is sized using the MATLAB algorithm. The number of stator slots is chosen taking into account the torque pulsation [16]. Furthermore, the best topologies of AFPM motor for low-power application is a 12/8 slot/pole, surface-mounted, single-sided configuration [9]. Designed AFPM motor specifications that satisfy the rated RFPM motor output characteristics are shown in Table 3.

Table 3. The designed AFPM motor specifications.

P_{out} [W]	66.6
T_{out} [Nm]	1.2
n_{rated} [min^{-1}]	530
Back EMF [V$_{peak}$]	15.75
I_{phase} [A$_{rms}$]	2.4
Number of phases	3
Slot/pole	12/8
Number of series turns (per phase)	344
Optimum λ	0.48
Inner diameter [mm]	56.9
Outer diameter [mm]	118.5
Magnet pole arc to pole pitch ratio	160/180
Permanent magnet	Ferrite
Winding type	Concentric

The design parameters are given in Table 3 for the new motor. Three-dimensional models of AFPM motors are required in order to do FEM analysis. Contrary to the radial motor, large changes in the axial axis and the axial path of magnetic flux in axial motors make 3D model and analysis unavoidable. A 3D FEM model is created in the same commercial software, Flux3D, to validate the analytical results.

3.2. AFPM motor analysis

The designed AFPM motor is modeled in the FEM-based package program shown in Figure 6a with the same materials used in the RFPM motor. The physical parameters and boundary condition are also identified.

Triangular prism elements are used for the mesh in that case (Figure 6b). The concentric windings are used as stator windings. The FEM-based AFPM motor analysis is carried out under both no-load and rated load conditions.

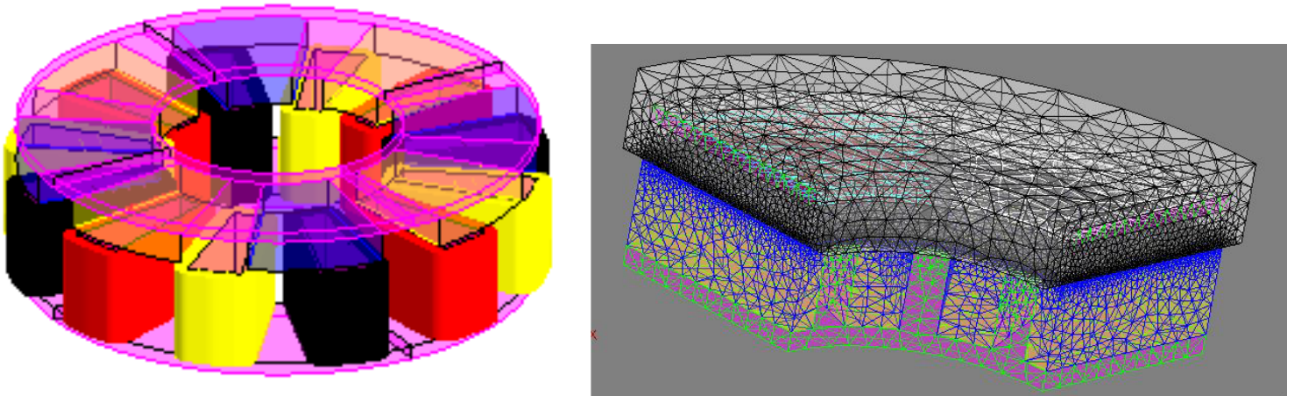

Figure 6. (a) AFPM motor structure (b) its mesh for a quarter model.

3.2.1. No-load AFPM motor operation

The no-load operation is done at a rated speed of 530 $\min^{-1}$, which is also the RFPM motor's rated speed, to validate the analytical AFPM motor design carried out by the MATLAB algorithm. The FEM and analytical results are given in Table 4. The coherency between the Back EMF results, with a 5.76% relative error rate, validates the analytical design.

Table 4. Comparison of AFPM motor back EMF.

	AFPM (analytical)	AFPM (FEM)	Relative error [%]
Back EMF [V_{rms}]	15.75	14.84	5.76

The AFPM motor design has the same electrical and magnetic loadings properties as the RFPM motor. The AFPM motor phase-to-phase back EMF at the rated speed is shown in Figure 7. The peak phase-to-phase induced back EMF of AFPM motor is calculated as 21.4 V. The FEM results for the AFPM and RFPM are given in Table 5. The results are also coherent, with a 4.7% relative error rate.

Table 5. Comparison of RFPM and AFPM motor back EMF.

	RFPM	AFPM	Relative error [%]
Back EMF [V_{rms}]	22.6	21.4	4.7

3.2.2. Rated load AFPM motor operation

The AFPM motor is designed according to the RFPM motor rated load conditions: 1.2 Nm shaft torque at 530 $\min^{-1}$ rated speed. Therefore, the load operation is carried out for a 1.2 Nm load at 530 $\min^{-1}$. The motor is driven by a six-switch inverter circuit with a square wave.

One of the constraints for the analytical design is the phase current. The objective was to keep the same current density for both motors. The phase current variation of the AFPM motor is given in Figure 8.

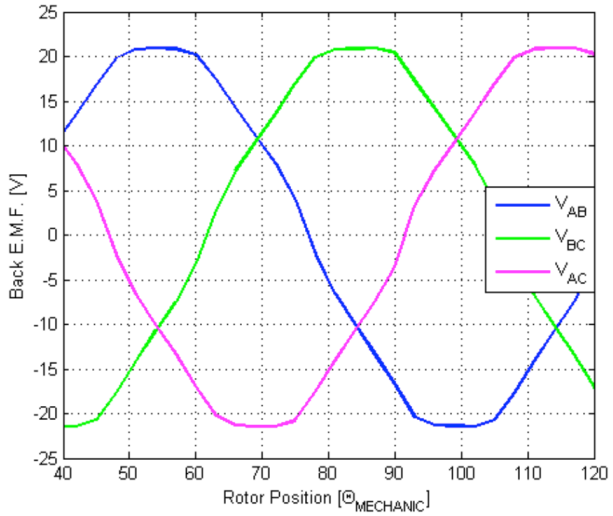

Figure 7. AFPM motor back EMF at a rated speed of 530 $\min^{-1}$.

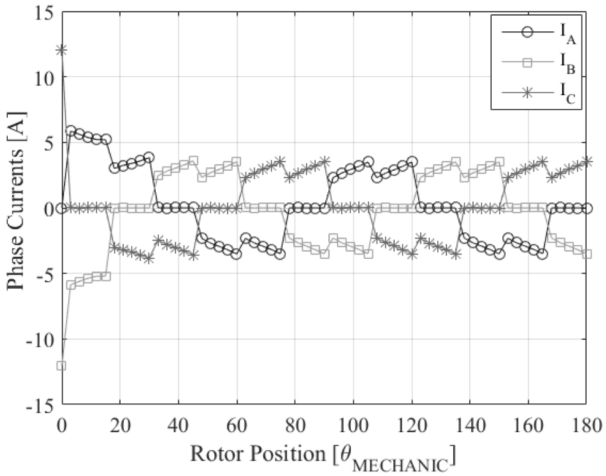

Figure 8. Phase currents of the AFPM motor at the rated load.

The analytical and FEM results of the phase current are given in Table 6. The motor shaft torque is shown in Figure 9. The average value of shaft torque is 1.173 Nm and the comparison with the analytical torque value is given in Table 7. When the torque profile given in Figure 9 is considered, the AFPM motor has a high amount of torque ripple, about 72%. This affects the average shaft torque in a negative way. The torque ripple can be reduced and the average torque can be increased.

Table 6. Phase current comparison of the AFPM motor.

	AFPM (analytical)	AFPM (FEM)	Relative error [%]
Current [A_{rms}]	2.4	2.305	3.96

Table 7. Average output torque comparison of the AFPM motor.

	Analytical	FEM	Relative error [%]
Torque [Nm]	1.2	1.173	2.25

3.2.3. Reduction of AFPM motor torque ripple

Torque ripple is the most important drawback of BLDC motors (Figure 9). Shaft torque consists of useful torque, cogging torque, harmonic torque caused by winding space harmonics, and harmonic torque caused by driver circuit harmonic currents. There are several ways to reduce torque ripple. Adjusting the magnet pole arc to pole pitch ratio is one method of reducing torque ripple and is applicable in the design step [14–20]. In the predesigned result of the AFPM motor given in Table 3, magnet pole arc to pole pitch ratio (α_i) is $160^\circ/180^\circ$. The magnet pole arc to pole pitch ratio is changed from $120^\circ/180^\circ$ to $170^\circ/180^\circ$ in 10° increments, while keeping magnet volume constant due to constant back EMF values. The torque and current versus magnet pole arc to pole pitch ratio of the AFPM motor driven at rated load condition are shown in Figure 10 and the comparison is given in Table 8. The required shaft torque is satisfied with the two magnet pole arc to pole pitch ratios: $120^\circ/180^\circ$ and $130^\circ/180^\circ$. The best design is $130^\circ/180^\circ$ due to the lower relative error of torque and phase current for 1.2 Nm shaft torque and 2.4 A phase current rated values. Torque ripple and average torque

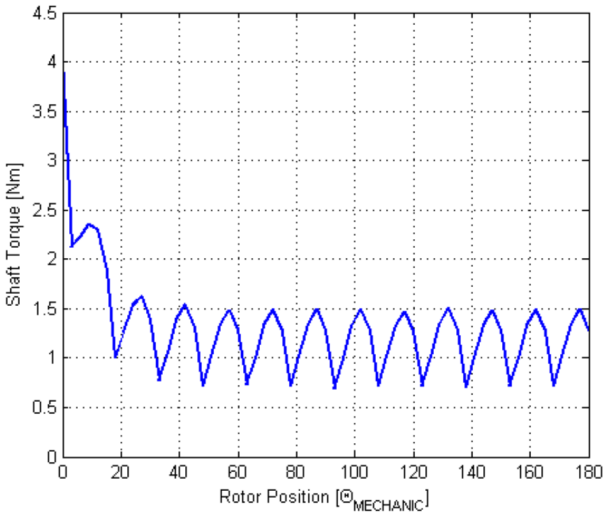

Figure 9. Torque characteristic of the AFPM motor.

are higher in the 120°/180° design; however, the phase current is also higher than 130°/180° and/or 2.4 A (the reference value). Higher phase current gives rise to lower efficiency due to higher copper losses in the stator windings. In addition, 1.204 Nm of torque can satisfy the required torque. As a result, torque ripple is reduced and the average torque is increased by tuning the magnet pole arc to pole pitch ratio to 130°/180°. The new designed AFPM motor has the same specifications given in Table 3, except for a 130°/180° ratio instead of 160°/180°. The shaft torque and phase current of the refined design of AFPM motor are shown in Figures 11 and 12, respectively. The results show that the 1.204 Nm AFPM motor shaft torque is in compliance with the required 1.2 Nm shaft torque (0.33% relative error rate) and phase current (1.67% relative error rate). Final analysis is carried out analytically for calculating AFPM motor losses and efficiency.

Table 8. Comparison of different AFPM motor magnet pole arc to pole pitch ratios.

(α_i)	T_{ave} [Nm]	T_{error} [%]	T_{ripple} [%]	I_{phase} [A]	I_{error} [%]
120°/180°	1.221	1.75	17.4	2.56	6.7
130°/180°	1.204	0.33	27.5	2.44	1.67
140°/180°	1.189	0.92	37	2.36	1.67
150°/180°	1.176	2	55.87	2.32	3.33
160°/180°	1.173	2.25	72	2.305	4
170°/180°	1.172	2.33	76.6	2.33	2.9

4. Comparisons of RFPM and AFPM motors

The designed AFPM motor and existing RFPM motor structures analysis results are compared in this section. The AFPM motor is designed for the best inner-to-outer diameter ratio λ, which gives the maximum power density. Later on, AFPM motor torque quality is improved by adjusting the magnet pole arc to pole pitch ratio. The magnet volume is kept constant while tuning the magnet pole arc to pole pitch ratio from 160°/180° to 130°/180°. Thus, the magnet axial thickness is increased; consequently, AFPM motor power density is changed.

Amount of AFPM and RFPM motors materials is given in Table 9. There is a difference between the

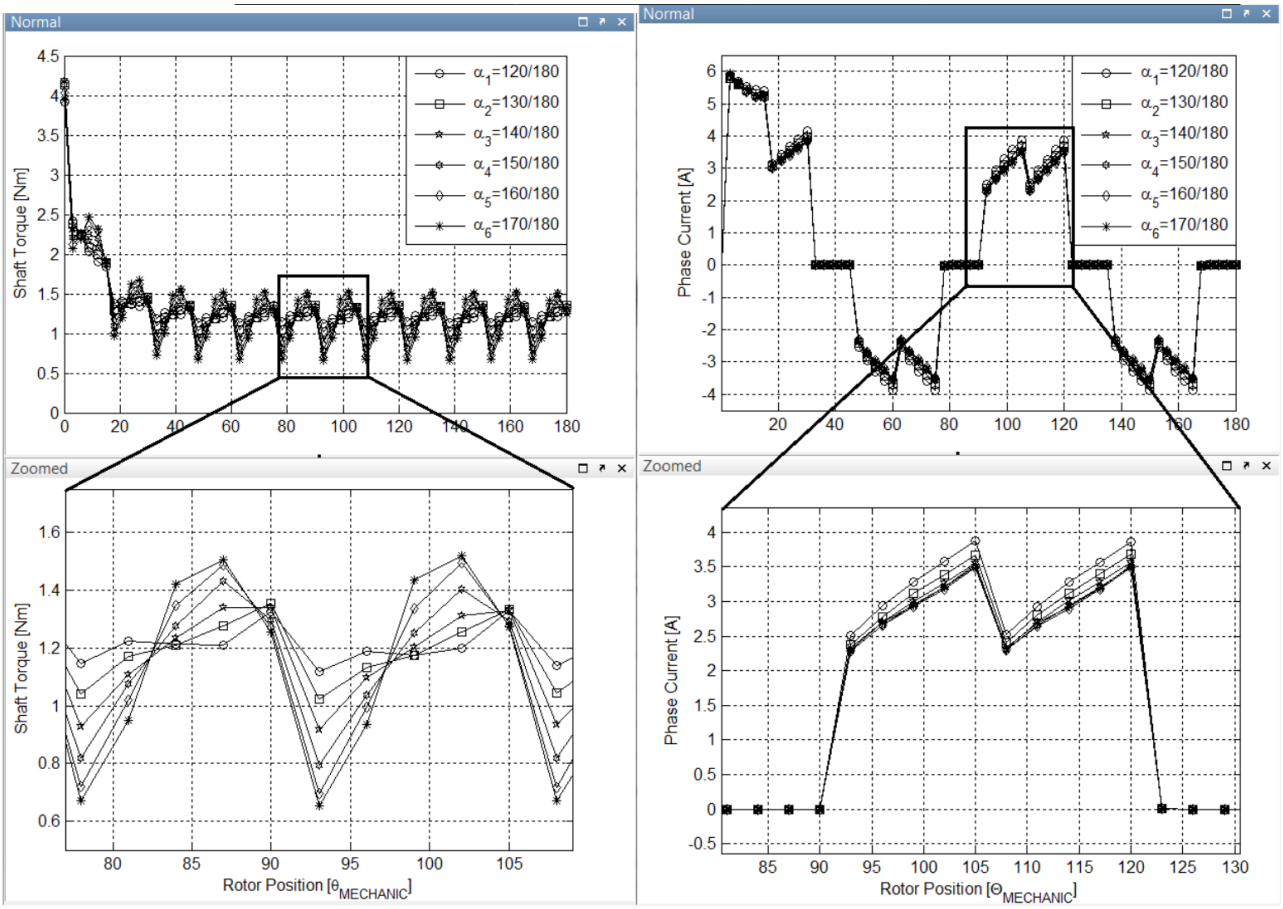

Figure 10. The AFPM motor shaft torque and current variation for different values of α_i.

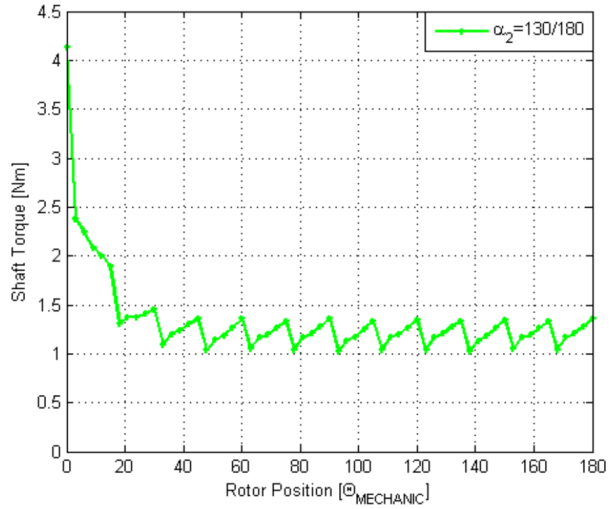

Figure 11. AFPM motor shaft torque at $\alpha_i = 130^\circ/180^\circ$.

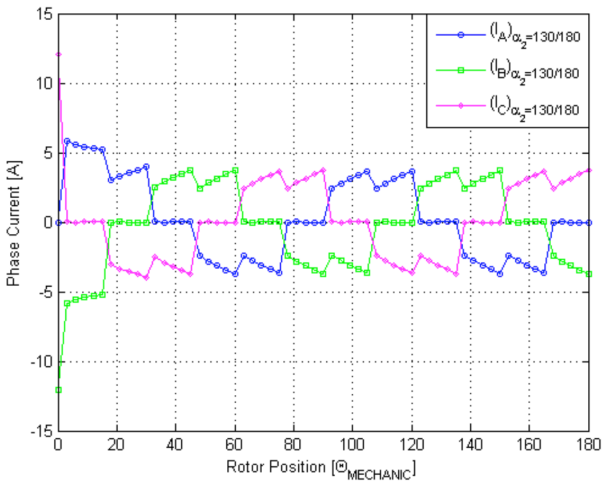

Figure 12. AFPM motor phase current at $\alpha_i = 130^\circ/180^\circ$.

materials, especially in the use of the laminated steel in the stator and rotor. The ferromagnetic materials are used with a higher utilization factor in AFPM motor. It results in a reduced amount of material. The

copper conductor is also decreased in the new design AFPM motor. Even though the number of series turns are increased in the AFPM motor, the copper weight is lower due to the compact structure of the AFPM motor. Mean turn length is substantially decreased in the AFPM motor results in this reduction. The permanent magnet amounts are nearly the same in both the AFPM and RFPM motors.

Table 9. RFPM and AFPM motor materials.

	RFPM	AFPM
Copper conductor [kg]	0.59	0.25
Stator lamination [kg]	3.31	0.93
Rotor lamination [kg]	0.65	0.17
Ferrite magnet [kg]	0.24	0.20

A second comparison is performed for power density, torque density, volume, weight, efficiency, and torque ripple. The detailed comparison is given in Table 10. AFPM motors have a 68.8% higher power density, 209.6% higher torque density, 40.6% lower volume, 67.6% less weight, 31.9% higher efficiency, and 50% lower torque ripple than RFPM motors. The AFPM motor surpassed all of the comparison headings, proving that it can be used in washing machine applications instead of the RFPM motor.

Table 10. Comparison of AFPM and RFPM motors.

	Power density [kW/m^3]	Torque density [Nm/kg]	Efficiency [%]	Torque ripple [%]	Volume [cm^3]	Weight [kg]
RFPM	85.25	0.251	52.67	55	781.3	4.79
AFPM	143.9	0.777	69.5	27.5	464.2	1.55

5. Conclusion

In this study, an AFPM motor analytical design algorithm is developed in MATLAB to maximize the power density. The algorithm is verified by using 3D FEM analysis of the AFPM motor. The RFPM motor and new designed AFPM motor met all specifications, such as power density, volume, weight, efficiency, torque ripple, and materials weight. According to this detailed study, for the same output specifications, less materials can be used in AFPM motor. The new designed AFPM motor has lower volume, less weight, and higher power density compared to the RFPM motor. Although an RFPM motor can be manufactured easily, an AFPM motor is a more attractive alternative because of the same output torque, back EMF for the same speed, and same current with less material and volume.

References

[1] Atherton WA. From Compass to Computer; A History of Electrical and Electronics Engineering. London, UK: The Macmillan Press Ltd., 1984.

[2] Chaker N, Salah IB, Tounsi S, Neji R. Design of axial-flux motor for traction application. JEMAA 2009; 2: 73-83.

[3] Hakala H. Integration of motor and hoisting machine changes the elevator business. In: Proceedings of the International Conference on Electrical Machines; 2000; 3: 1242-1245.

[4] Profumo F, Zhang Z, Tenconi A. Axial-flux machines drives: a new viable solution for electric cars. IEEE Trans Ind Electron 1997; 44: 39-45.

[5] Mebarki A, Gerada D, Brown NL. Analysis of an axial PM machine with field weakening capability for engine integration. In: Proceedings of 7th IET International Conference on Power Electronics, Machines and Drives; 2014; 1: 1-6.

[6] Zhang Z, Profumo F, Tenconi A. Axial flux versus radial flux PM machines. Electromotion 1996; 3: 23-29.

[7] Simsir NB, Ertan HB. A comparison of torque capabilities of axial flux and radial flux type brushless DC (BLDC) drives for wide speed range applications. In: Proceedings of IEEE; 1999; 2: 719-724.

[8] Nakahara A, Deguchi K, Kikuchi S, Enomoto Y. Comparative electrical design of radial and axial flux permanent magnet synchronous machines under space limitation. In: Proceedings of the International Conference on Electrical Machines; 2014; Berlin, Germany. 1: 422-428.

[9] Sitapati K, Krishnan R. Performance comparisons of radial and axial field, permanent magnet, brushless machines. IEEE T Ind Appl 2001; 37: 1219-1226.

[10] Gieras JF, Wang RJ, Kamper MJ. Axial flux permanent magnet brushless machines. Berlin, Germany: Springer Science & Business Media, 2008.

[11] Honsinger VB. Sizing equations for electrical machinery. IEEE T Energy Convers 1987; 2: 116-121.

[12] Huang S, Luo J, Leonardi F, Lipo TA. A comparison of power density for axial flux machines based on general purpose sizing equations. IEEE T Energy Convers 1999; 14: 185-192.

[13] Parviainen A, Niemelä M, Pyrhönen J. Analytical, 2D FEM and 3D FEM modelling of PM axial-flux machines. In: Proceedings of the 10th European Conference on Power Electronics and Applications; 2003; Toulouse, France. 3: 1955-1961.

[14] Ertuğrul Donmezer Y. Reducing torque ripples in brushless direct current motors. MSc, İstanbul Technical University, İstanbul, Turkey, 2009.

[15] Aydin M, Huang S, Lipo TA. Design and 3D electromagnetic field analysis of non-slotted and slotted torus type axial flux surface mounted permanent magnet disc machines. In: Proceedings of the IEEE International Electric Machines and Drives Conference; 2001; Cambridge, MA, USA. 1: 645-651.

[16] Hendershot JR, Miller TJE. Design of Brushless-Permanent Magnet Motors. Oxford, UK: Magna Physics Publishing & Clarendon Press, 1994.

[17] Parviainen A, Niemelä M, Pyrhönen J. Reduction of torque pulsations in axial-flux interior PM synchronous machines. In: Proceedings of the Nordic Workshop on Power and Industrial Electronics; 2002; Stockholm, Sweden.

[18] Donmezer Y, Ergene LT. Skewing effect of interior type BLDC motors. In: Proceedings of the XIX International Conference on Electrical Machines; 2010; pp. 1-5.

[19] Zhang Z, Profumo F, Tenconi A. Design of an axial flux interior PM synchronous motor with a wide speed range. In: Proceedings of the International Conference on Electrical Machines 1996; 3: 273-278.

[20] Caricchi F, Crescimbini F, Santini E. Basic principle and design criteria of axial-flux PM machines having counter-rotating rotors. IEEE T Ind Appl 1995; 31: 1062-1068.